JOURNAL OF MATERIALS SCIENCE 30 (1995) 2706–2715

Deformation microstructures and the shear strain rate of type 304 stainless steel sheet in cylindrical deep drawing of warm working

J. S. CHANG, S. S. CHOU
Department of Materials Science and Engineering, (22) National Cheng Kung University, Tainan, Taiwan 70101

A deep-drawing test was conducted under a single temperature or two temperatures on both sides of type 304 stainless steel sheet, 0.8 mm thick. The different results produced by these processes are described. A lower rate of shear straining is generated at 100 °C in the two-temperature process than in the single-temperature process, and a much larger rate is produced with room-temperature working. Their microstructures at the failure point and the flange portion nearing the die throat were studied by optical microscopy and TEM. An intermixed structure of lath and blocky α'-martensites appeared at the failure point in cold working. By warm working at a single temperature, homogeneous shear in a single direction and coarser slip bands were generated. Heterogeneous shear straining on both sides of the specimen occurred in the two-temperature process, and the microstructure of the failure point was observed as twin–twin intersections. The microstructures generated in the flange portion corresponding to the individual process, appeared to be blocky martensite nucleation and growth at the shear band intersections, twin–twin band or twin–slip band intersections, respectively. The strengths of these microstructures at different positions are compared with each other and the drawability is explained.

1. Introduction

In the deep-drawing process, the drawability of a metal sheet, usually, could be evaluated by the value of the limiting drawing ratio which depends on the characteristics of the material. The effect of anisotropy and work-hardening features of the sheet metal on the punch force during the deep-drawing performance, have been treated by a approximate method [1–4]. Both the representative values of material characteristics could also be applied to the calculation of stress and strain distributions and the punch force in deep drawing of a cup [5, 6]. The punch forces are higher for smaller values of plastic anisotropy. The limiting drawing ratio can be determined under the condition where the punch force required for drawing a cup had exceeded the force causing the instability along the wall of a drawn cup. It has also been described that the limiting drawing ratio increased linearly with increasing plastic anisotropic value, and increased slightly with increasing work-hardening coefficient.

When steel sheets were processed by cylindrical deep drawing, their drawability was also influenced by the temperature on the sheet specimen. The tensile strength of the material at the punch shoulder portion must always be larger than that at the flange portion, so that the drawability could increase appreciably, or it will fail from that point. This effect could be established by suitably controlling the temperature difference between the punch and die, that is, the drawability of sheet metals can be improved by keeping the temperatures of the punch and die at a appropriate difference during the deep-drawing performance. The dependence of the forming height of a drawing cup on the punch and die temperature was discussed by Tetsuro *et al* [7]. The success or failure of deep drawing due to the temperatures of the punch and die, and the reason why drawability increased in the warm-working condition, were explained by the tensile-strength increased in the area of the punch shoulder and is always large compared with that at the flange portion.

Type 304 stainless steel can induce the martensite transformation by plastic deformation at room temperature. Its strain hardening and deformation rates are rapid and increase with decreasing temperature. Once the saturation of martensite has occurred, the rate of work hardening decreases more quickly and results in necking. In biaxial tension, the ductility of type 304 stainless steel is low and can be explained by this high transformation rate associated with the faster tendency towards plastic instability [8]. But the $\gamma \rightarrow \alpha'$ transformation can be sufficiently suppressed at high strain rates due to the temperature increase resulting from adiabatic heating. This implies that when the material is heated to a certain temperature level during plastic deformation, the martensite transformation will not be generated.

0022–2461

The 304 stainless steel sheet always fails during deep drawing at room temperature. However, its drawability can be improved by a complex process with heating in the die and cooling in the punch. A microstructural study on this material is presented in the present paper. The purpose of the present work was to examine the deformation products generated from the different processes of deep drawing, and by a comparison of those results to check which type of deformed structures may influence the drawability of this material.

2. Experimental procedure

The nominal composition of type 304 stainless steel in this experiment was 0.06% C, 0.63% Si, 1.09% Mn, 0.03% P, 0.03% Cu, 0.01% S, 0.12% V and 8.63% Ni, 18.12% Cr, and the balance iron. The disc-shaped sheet specimens, 110 mm diameter and 0.8 mm thick were subjected to deep-drawing at temperature 25 °C, or at 100 °C with and without the 50 mm diameter punch, and cooled by pumping iced water through the drilled centre axis. This is termed a two-temperature process to represent warm working by which the die is heated and the punch is cooled; while the single temperature process indicates only heating or cold working were performed.

For a fixed process, the specimens were incrementally drawn into a cylindrical cup of different depths by the flat-ended punch. For the same processing temperature, the thickness at the failure point of the cups at different drawing depths was measured. Even though cups were produced under different conditions, it was noticed that the failure point of the specimen was located at same position relative to the rolling direction of the original sheet specimen, therefore the specimens were sliced by the electric spark erosion method into pieces 2 mm wide for optical microscope observation, and into discs 3 mm diameter for examination by transmission electron microscopy (TEM).

The sliced specimens for optical microscope observation were first immersed in 10% oxalic acid and electrically etched for 45 s at 6 V d.c. with a stainless steel plate serving as the cathode. This procedure was then repeated in 50% nitric acid for 2 min at 1.5 V d.c. The discs intended for examination by TEM were worn down equally on both surfaces to a thickness of 0.20–0.25 mm, and then twin-jet polished in a solution containing 10% perchloric acid and 90% acetic acid at a voltage of 20 V d.c. to produce the TEM foil specimen.

Another specimen located at the flange portion near the die throat was also prepared for TEM observation by a similar method. The features of the deformed structures were identified from the selected-area diffraction patterns in the TEM.

3. Results

3.1. The rate of shear straining

When specimens were incrementally deep drawn at a fixed condition to different depths, the thickness strains at the failure point were measured and calculated as $(S_0 - S)/S$, where S_0, S represent the original and current thickness value of the sheet specimen and the failure point, respectively. They are plotted against the corresponding drawing depth as shown in Fig. 1. At room temperature, a smaller range of drawing depths was associated with a much larger strain value. At 100 °C in the single temperature process, the shear strain is reduced but still exists within a small range of drawing depth. However a much smaller strain value, associated with greater range of drawing depths, is generated in the two-temperature deformation process at 100 °C. This indicates that warm working at two temperatures produces the lowest rate of shear straining in this experiment, warm working in a single temperature yields the intermediate rate of shear straining and a smaller drawing depth indicating that its has been produced a result of poor drawability. For room-temperature working, the highest ductility and a much higher rate of shear straining is still seen, but the specimen will quickly fail during necking.

3.2. Optical metallography

In order to obtain the macroscopic deformation behaviour in this material, the position from which failure always originated was subjected to optical observation. Different processes of deformed grain structures were viewed from the longitudinal cross-section so that the occurrence of straining on both sides could be observed on the same micrograph. In cold working, it is noted that all of the grains have strained to a large degree, and nearly all of the grains have a dark region on them, as shown in Fig. 2a. This might be the structure of α' martensite which can be later identified by TEM examination in this experiment.

For elevated single-temperature deformation (the optical micrograph shown in Fig. 2b), all of the grains deformed in a fairly uniform way and were elongated along one direction parallel to the punch force. Easy gliding took place between every grain so that little resistance existed between them, and much more shear straining was created during plastic deformation.

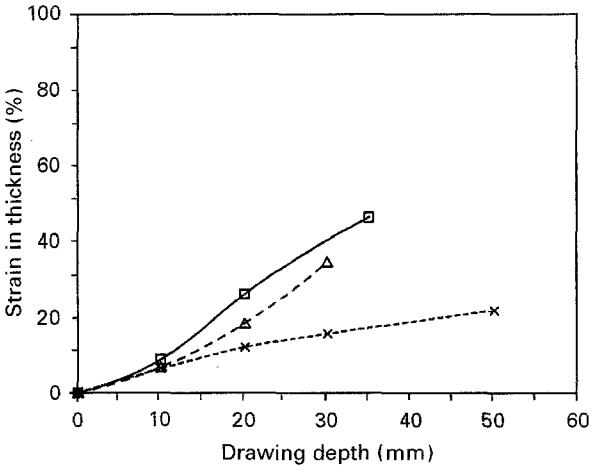

Figure 1 The rate of shear straining relative to drawing depth, (□) at room temperature, (△) at 100 °C in the single-temperature process, (X) at 100 °C in the two-temperature process.

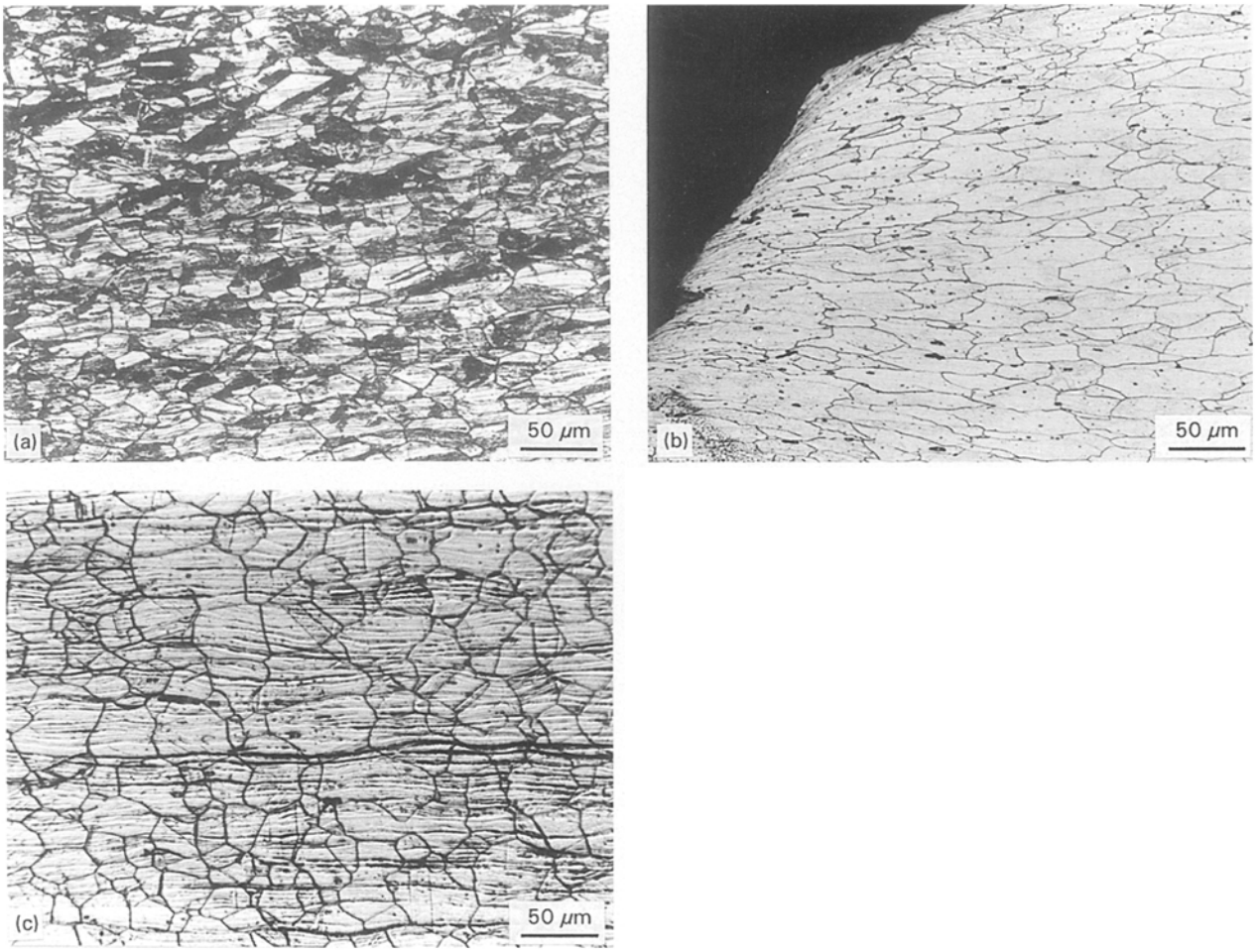

Figure 2 Optical micrographs viewed from the longitudinal cross-section of the failure point: (a) at room-temperature working, (b) at 100 °C of single-temperature working, (c) at 100 °C of the two-temperature deformation.

When deformation was performed by a two-temperature process, that is, keeping the inner side at a cooling temperature, 2 °C, and the outer side at a heating temperature, 100 °C, the deformed structure was observed as irregular-shaped grains in a manner of bi-axial stress and of unequal size, see Fig. 2c. In this case, the grains in contact with the outer side of the drawn cup as seen in the lower part of the micrograph, were less deformed than those nearing the inner side, as viewed from the longitudinal cross-section. This indicates that those grains had been arranged non-uniformly in more slip directions due to the different temperatures acting on the both sides of the specimen. When deformation proceeded, gliding resistance had been generated between each grain, so that they glided along in more than one direction and were not easily elongated. This phenomenon of non-uniform arrangement between every grain exhibited the effect of lowering the shear strain rate.

3.3. TEM study at the failure point

The macro-deformed structure along the longitudinal axis of the failure point has been examined by optical microscopy as stated above. The microstructure was then studied by transmission electron microscopy at the same failure point position. TEM specimens, 3 mm thick, were taken from two positions on the cup wall: one was located at the failure point described above, the other was from the flange portion nearing the die throat. These two portions suffered different states of stress, which will influence the drawing of material into the die. In other words, the drawability depends on whether the tensile strength of the failure point, which always occurs at the punch shoulder, is greater than that of the flange portion. If the strength of a highly stressed failure point is large enough in the period of deep drawing, the specimen can achieve a better drawability.

The results of the TEM examination of deep-drawn specimens at the failure point, which had deformed to the largest depth corresponding to the individual process, are shown in Figs 3–5. For room-temperature working, a strain level of 0.462 at a drawing depth 35 mm was found, and its microstructure consists of lath and intermixed blocky martensites, as shown in Fig. 3. Fig. 3a shows the bright-field image in a $\langle 1\,1\,0 \rangle$ zone; strain-induced martensite was formed at the failure point. It also shows much more dense dislocations piled up around the martensite caused by the plastic deformation strain. A $\{1\,1\,1\}$ reflection of a dark field is presented in Fig. 3b, the $(\bar{1}\,1\,\bar{1})$ of the γ matrix is converted into the $(0\,1\,\bar{1})$ of bcc α' martensite product, which is consistent with the Kurdjumov–Sachs (KS) relationship. Fig. 3c and d show the diffraction pattern and its identification.

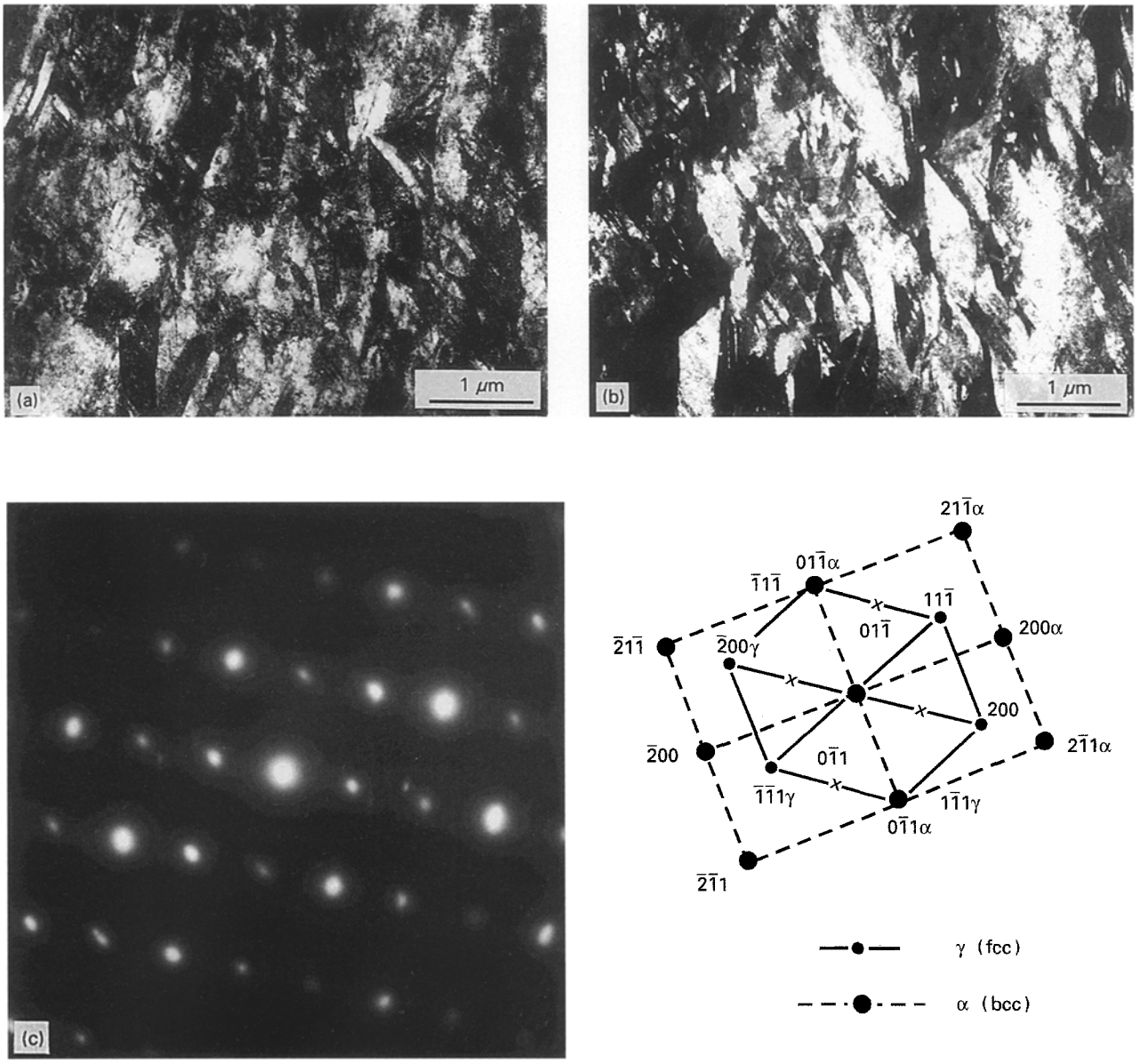

Figure 3 Transmission electron micrograph of the failure point at room temperature, (a) bright-field image, (b) dark-field image of $(0\,1\,\bar{1})$ reflection, (c, d) diffraction pattern and its identification.

The hardness increases due to the presence of strain-induced martensite, and its more seriously straining will easily cause localized instability.

The microstructure of the specimen deformed in the 100 °C single-temperature process is shown in Fig. 4. It has strain value 0.346, corresponding to a drawing depth of 30 mm, and the rate of shear straining is reduced. The microstructure is observed to be coarse dense dislocation walls on the (1 1 1) plane of γ matrix, which glided in a single slip system. Obviously, the number of intersections of shear bands is greatly reduced at elevated temperature, but the shear strain rate is still large, so the slip bands were generated by the shear stress and propagated rapidly on further straining. It also shows one dense dislocation wall is less dense than another, indicating that a small misorientation has existed between them.

Under two-temperature deformation in warm working, the specimen had a strain level of 0.215 and a drawing depth of 50 mm. Fig. 5a shows the TEM bright-field micrograph at the failure point. Twins in two variants are presented on conjugate $\{1\,1\,1\}$ planes as identified by the SAD diffraction pattern in Fig. 5b. One group of twins has formed on the primary slip system, and another on the secondary slip system, and they have intersected each other somewhere in the micrograph. This process with different temperatures on both sides of the specimen, will greatly cause different slip systems to be active from both sides during deep-drawing. These two systems meet at the mid-thickness of the cup wall and will impinge on each other, finally intersecting two twin variants formed in either slip plane and crossing one another. It is noticed that this type of microstructure lowers both the strain value and the rate of shear straining at the punch shoulder position.

3.4. Transmission electron micrographs at the portion nearing the die throat

The plane stress at the flange portion, when the specimen had suffered both radial and circumferential

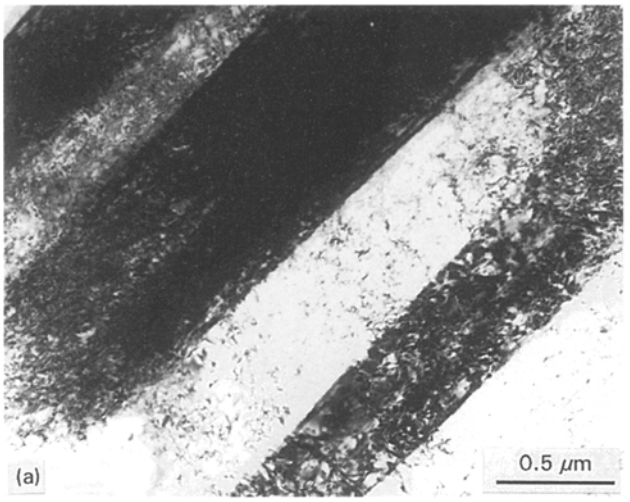

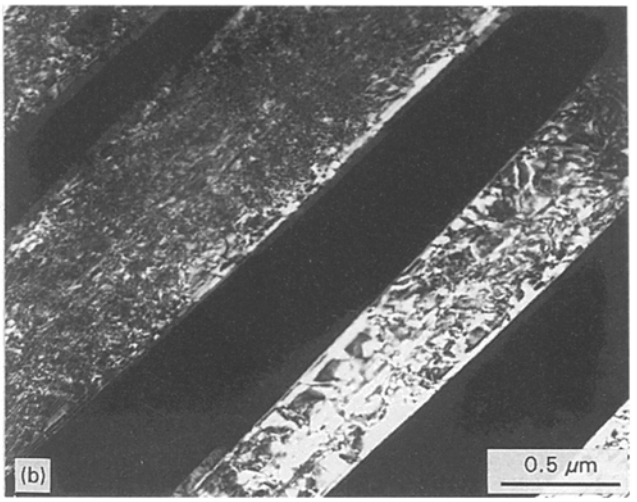

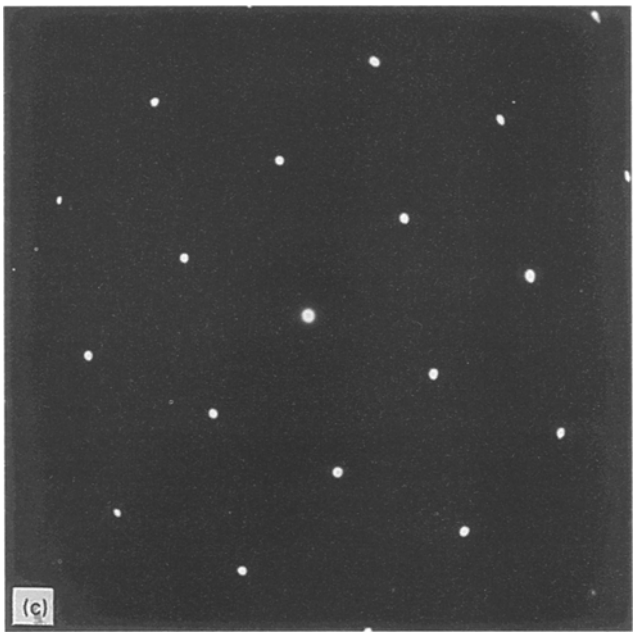

Figure 4 Transmission electron micrograph of the failure point at 100 °C of single-temperature working: (a) bright-field image, (b) dark-field image of (1 1 1) matrix reflection, (c) its diffraction pattern.

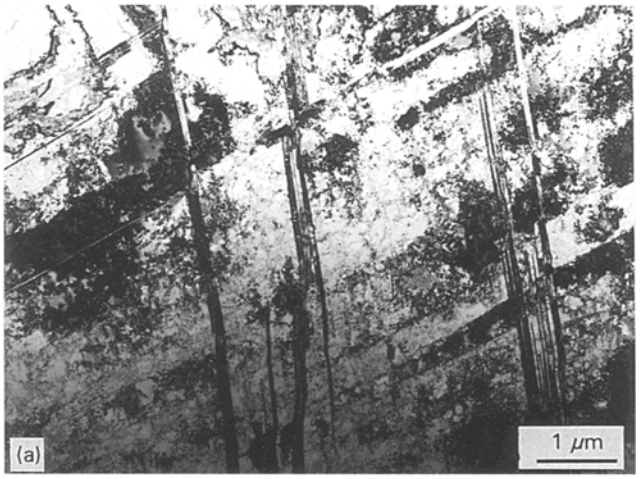

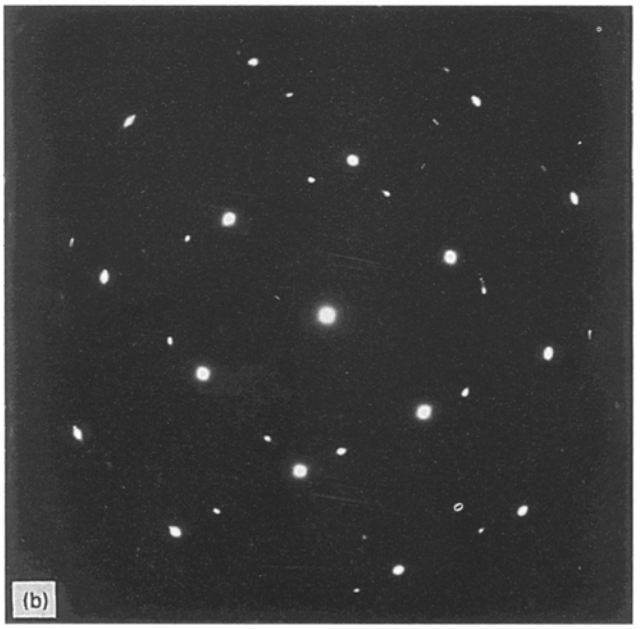

Figure 5 (a) TEM bright-field micrograph at the punch shoulder performed by two-temperature deformation of 100 °C, and (b) its diffraction pattern.

stresses, just reached the position nearing the inlet curvature of the die but was not drawn into the die. The microstructures of a specimen nearing the die throat for the different processes are shown in Figs 6 and 7.

Under the process of room temperature working, many more shear band intersections appeared and acted as nucleation sites for α' embryos, as shown in the bright-field micrograph in Fig. 6a. Very little martensite was created and the dislocations did not accumulated to a large extent, as produced at the failure point. Lath martensites were not observed in this region. Fig. 6b shows the dark-field image of a $\{1\,1\,0\}$ reflection in the zone axis $\langle 1\,0\,0\rangle$ of bcc α' martensite and Fig. 6c is the dark-field image of an ε shear-band reflection; Fig. 6d and e show the diffraction pattern and its identification, respectively. The blocky α' martensite is formed at the shear-band intersections, and appeared in the dark-fields of both the shear bands. This indicates that the growth process of α' martensite involves the coalescence of embryos that were nucleated from both slip systems. α' had also grown from the slip plane and formed an irregular blocky martensite, as seen in Fig. 6a.

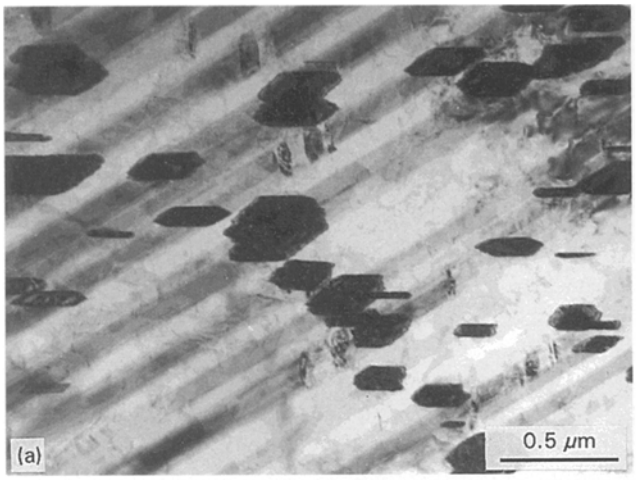

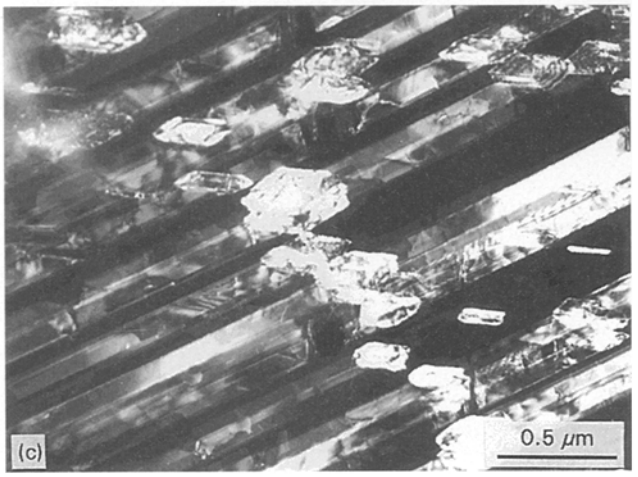

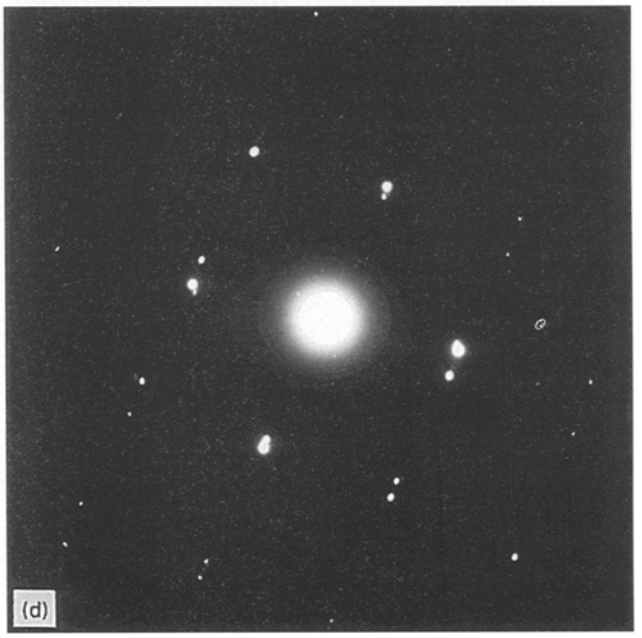

Figure 6 Transmission electron micrograph of the flange portion at room-temperature working: (a) bright-field image, (b) dark-field image of (1 1 0) bcc martensite reflection, (c) dark-field image of an ε slip band, (d) the diffraction pattern and its identification (e).

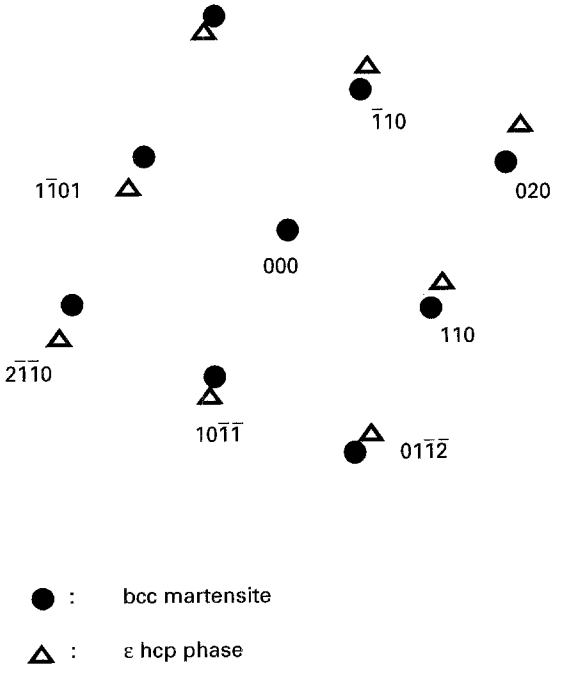

The microstructures were observed to be twin–twin band intersections, and twin–slip band intersections in the one- or two-temperature processes at 100 °C, respectively; both are shown in Fig. 7a and b. For one-temperature deformation, Fig. 7a shows the TEM bright-field image of twins and parallel-edged twin band formed on two conjugate {1 1 1} planes. The twin band had been penetrated by the crossing twins and was bent and cut off at the intersection when it propagated. This indicates that the twin band is unstable and of such poor strength that it had been bent by the compressive circumferential stress and was interrupted at the highly stressed intersection on further straining.

A more stable type of microstructure appeared in the form of twin-slip band intersection in two-temperature straining. These twins were divided into two categories and are individually distributed on opposite sides of the slip band; in fact, up or down on the slip band, as shown in Fig. 7b, both the slip band and micro-twins have appeared. The dark-field image of the twins on the {1 1 1} reflection in the ⟨1 1 0⟩ zone and its diffraction pattern are shown in Fig. 7c and d, respectively. The slip band has been offset by the crossing twins, as seen from Fig. 7f, which is the dark field of the {2 0 0} reflection in the ⟨1 0 0⟩ zone axis of Fig. 7e.

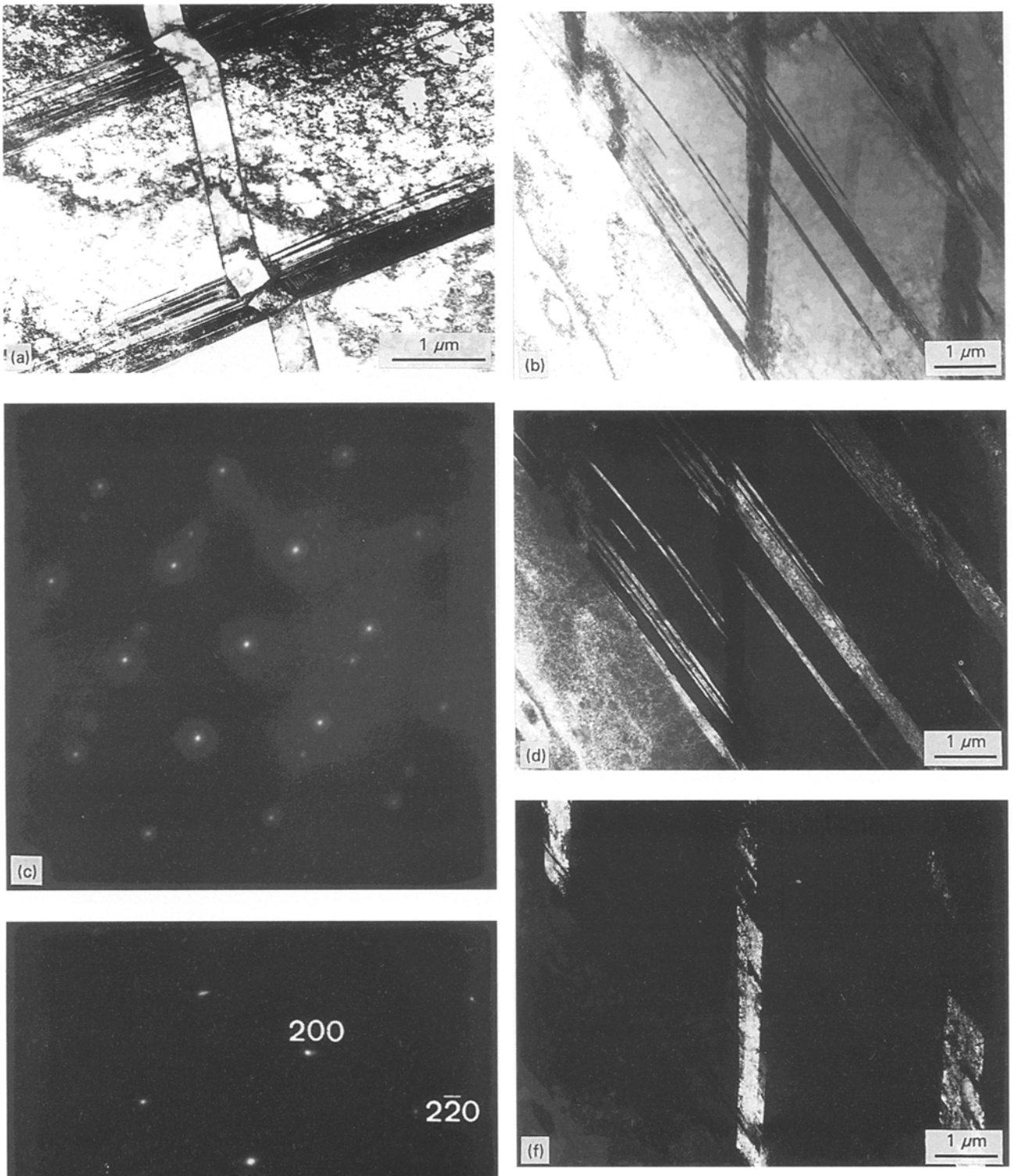

Figure 7 Transmission electron micrograph of the flange portion at 100 °C warm working: (a) bright-field image at single-temperature deformation, showing the intersections of twins and a parallel-edged twin band, and (b) intersections of twin and slip band appearing for deformation, two-temperature (c) twinning diffraction pattern, and its dark-field reflection on (1 1 $\bar{1}$) is shown in (d); (e) diffraction pattern in [0 0 1] zone axis of the matrix, and the dark-field image of the (2 0 0) reflection is shown in (f).

4. Discussion

From the results of this experiment observed in optical microscope and TEM, it was found that the number of shear band intersections apparently decreases with increasing temperature, and the rate of work hardening is then reduced. Thus, its tensile strength is low under punch-drawing conditions. At room temperature, the higher number of shear band intersections in type 304 stainless steel, have contributed to the production of α' martensite, because α' martensite is nucleated at the intersections of shear

bands and appears at lower strain levels leading to the enhanced work-hardening behaviour of metastable austenitic stainless steels. At the failure point at which martensitic transformation occurs, there are so many more nucleation sites that the lath martensite coalesced to produce the blocky structure. α' martensites behave as hardening bodies and as accelerators for the storage of dislocations in the austenite phase. They also act as obstacles to slip, resulting in an increased dislocation density in the austenitic phase. Once the saturation of martensite transformation has been reached, the work-hardening rate will soon decrease and result in premature necking. Thus, in deep-drawing, the higher shear strain rate of 304 stainless steel might be explained by the tendency for α' martensite saturation rapidly occurring at room temperature, and leading to a decreased strain-hardening rate and premature instability.

Less straining of γ and a decrease in the percentage of α' has occurred if the process temperature is increased. Because the temperature rise was insufficient to suppress the $\gamma \rightarrow \alpha'$ transformation. The martensite effect is eliminated at 100 °C, but the work-hardening rate is much lower due to the remarkable reduction of shear band intersections in the single-temperature process. This causes a rapid rate of shear straining even though a reduced strain in the thickness has been produced.

At temperatures above the M_d (room temperature) [9], the yielding is entirely by slip of the austenite; homogeneous deformation seems to occur preferentially in the single-slip system and coarse growth occurs for further straining. The coarse dense dislocation walls glide in a uniaxial direction, and the accumulated internal stress cannot be relieved in the period of plastic deformation, thus it sheared along the direction of the applied stress and caused the faster shear strain rate. Thus, homogeneous plastic deformation will easily promote shear instability.

A too high rate of work hardening at room temperature will cause a high shear strain rate, due to martensite transformation. A much lower rate of work hardening at 100 °C also leads to a large rate of shear straining, because of the unrelieved internal stress existing in the grains. Therefore, an optimum rate of work hardening with strain is required for extensive drawability in this unstable austenitic steel. The work-hardening rate must be great enough to prevent the onset of shear instability but not too large, because excessive transformation will induce early fracture in the less ductile martensite [10, 11].

The internal stresses due to pile-up of dislocations could be relaxed by effective slipping on secondary system, and this may increase the forest dislocation density during deformation [12]. Only the most highly stressed secondary systems of fcc crystals produce reactions with primary dislocations to form Lomer–Conttrell dislocations which act as one kind of stable structure [13]. These secondary systems could be activated by cooling in the punch side while it was heated in the die, as took place in this experiment. Because of the temperature difference on both sides of specimen, most of the grains deform to a different degree, as shown in Fig. 2c viewed from its longitudinal cross-section. The larger size of grains located near the punch side, indicates that the strain on the inner surface is lower than at the smaller grains nearing the outer surface. It also implies that different strains are present on both sides. Likewise, as shown in Fig. 2b, both sides have suffered the same strain because homogeneous shearing in the longitudinal direction is observed. By comparing these two cases, the biaxial features of the grains generated in the two-temperature process viewed along the longitudinal direction indicate that at least two stress directions have acted on both sides of the cup, while the preferential shear stress in a single direction is present in the one-temperature process. Thus, the dislocation lines may slip in more than one slip system and will impinge on each other as they deform under different strains from both sides. The slip lines of the first slip system will act as obstacles to the conjugate system and lead to grains strong enough to resist the shear instability. It is obvious that the rate of shear straining and the strain value in the thickness is greatly reduced, and its plastic anisotropy will then be increased. In polycrystalline metal, the anisotropy increase will generate large stresses in the grains, but these stresses can be relieved by twinning intersections.

In the two-temperature process, the primary slip dislocations intersect a secondary slip dislocation to produce a jog of sufficient length to make it a twin source in this work-hardened crystal. Twinning propagated in this manner depends upon twinning planes that were active. Homogeneous deformation took place on one side, while on the other side it deformed heterogeneously with the former; in addition, the deformation on one side took place on a different twinning plane from that on the other side. Jogs produced by primary slip dislocations are sources of twins on the primary twin plane, and twins on the secondary twin plane occur in a similar way. The two active planes are related as conjugate twinning planes. Thus when the internal stresses are the same in both systems, conjugate twin–twin intersections will be formed on both conjugate planes.

In the flange area, under the combined action of radial and circumferential stresses, stresses exhibit tensile and compressive characters, respectively, and a great difference in the directions of stresses are obviously presented. This will cause dislocations to glide in two slip systems intersecting with each other to form dislocation cells, and Lomer–Cottrell locks might be formed during plastic deformation. These dislocation cells are not necessary for a stable structure, as observed from this experiment, because the cell boundaries can be modelled as a planar obstacle of finite thickness in which the boundary can trap edge or screw dislocations [14]. Those boundaries trapping edge dislocations or trapping screw dislocations will decide whether the cell structures will be the most or the least stable. At one-temperature deformation, homogeneous shear straining on both sides of the specimen occurred under the same flow stresses, the boundaries of the dislocation cell trapped screw dislocations and were unstable, and those screw

dislocations meeting the boundaries may have produced cross-slip instead of traps, so a twin band was easily created by the radial tensile stress. In another direction, twinning occurred on the secondary system due to the compressively circumferential stress which is more stable, and might be generated by the extension of the prismatic source [15] in the same period as the twin-band propagation.

In two-temperature deformation, heterogeneous shear straining occurred at the flange portion nearing the die throat, which modulated the straining state to accommodate the different strain paths on both sides. The cell structures created during this heterogeneous process were subjected to different strains on both sides of the specimen, and different stresses are generated, and thus boundaries may trap edge dislocations that are very stable. The phenomenon of twin-band formation will not take place in this process.

During the room-temperature process, α' martensite is nucleated at shear-band intersections which were produced by the radial and circumferential stresses. Similar to the biaxial tension [16], there are also many more shear-band intersections created at this combined tensile and compressive stressed state, which act as nucleating sites for bcc α' martensite transformation. As the temperature increased, the thermodynamic driving force was reduced and tended to lower the probability of the nucleation of martensitic embryos. Twins were formed at 100 °C in two-temperature deformation, and distributed up and down the slip band, as shown in Fig. 7b; this could be explained by the operation of a prismatic twin source mechanism [17] in which a long jog was created and acted as a twin source.

On comparing the transmission electron micrographs of the failure point with that of the flange portion for room-temperature working, the intermixed structure of lath and blocky martensites shows a tendency to be less stable than the simple irregular blocky martensite. Fig. 3 shows the intermixed martensites at the failure point, the (1 1 1) of γ matrix is converted into the (1 1 0) of α' martensite, which corresponds to the KS relationship. The irregular blocky martensite produced at the flange portion as shown in Fig. 6, has the bcc pattern of the $\langle 1\,0\,0 \rangle$ zone axis, indicating the Nishiyama (N) relationship holds. These results agreed with that described by Mangonon and Thomas [16], the transformed bcc crystal formed first in the N orientation, and KS is the final orientation between the γ and α'. The intermixed martensite is associated with piled-up dislocations, implying that the saturation of martensite is generated and will quickly result in necking. It is beyond doubt that this intermixed structure produced at the failure point is less stable than the initially formed blocky martensite at the flange portion. In this condition, the punch force applied for drawing a cup will easily exceed the tensile strength of the cup wall, the position at which failure took place.

In a similar way, the coarser structure of dense dislocation walls gliding along a single direction, observed at elevated temperature, is less stable than the intersections of microtwins and twin bands. Shear instability will also take place from there, if the punch force is large enough. Twin–twin intersections have been created in the two-temperature process, which is one type of a more stable structure as compared to the twin–slip band intersections. The tensile strength of the punch shoulder with this structure is large enough to resist the punch force and allows shear instability to take place with difficulty, compared to that produced at the flange portion.

If a special combination of the twin–twin and twin–twin band intersections existed at the corresponding portion, as found in this experiment, it could be inferred that the cup might cause failure at the portion nearing the die throat. This case can be envisaged as taking place in the two-temperature process with sufficient cooling at the punch shoulder portion and insufficient cooling at the die throat.

5. Conclusions

1. When type 304 stainless steel sheet is subjected to a deep-drawing test, the rate of shear straining at the punch shoulder portion relative to drawing depth is highest for room temperature working. This can be reduced by increasing the process temperature and the best result is generated for two-temperature deformation of warm working in this experiment.

2. At room temperature, much more shear strain is produced and the transmission electron micrograph at the failure point shows intermixed lath and blocky martensite. This structure is less stable than the simple blocky martensite created at the flange portion. The premature local plastic instability will be generated there due to its much higher rate of work hardening.

3. At 100 °C of the single temperature process, the steel is strained by homogeneous shearing, and coarser dense dislocation walls gliding in a single direction are observed by TEM at the failure point. This structure is also less stable than the intersections of twins and twin bands generated in the flange portion. Because the number of intersecting shear bands decreased as the temperature increased and caused a remarkable reduction in work-hardening rate, the rate of shear straining is still large, implying that it has poor drawability.

4. At 100 °C in the two-temperature process, heterogeneous deformation occurred as seen along its longitudinal axis by optical microscopy. The transmission electron micrograph at the punch shoulder is observed as twin–twin intersections. This appears to be a much more stable structure on comparing with the twin–slip band intersections generated at the flange portion. A smaller strain value and much lower rate of shear straining are both meaningful in that they will lead to better drawability in this process.

Acknowledgements

The provision of the deep-drawing equipment by Metal Industry Development Center is acknowledged, and we thank Mr S.K. Chang for the assistance with apparatus performance and die assembling during the deep-drawing test. This work was financially supported by the National Science Council.

References

1. R. L. WHITELEY, *Trans. ASM* **52** (1960) 154.
2. M. FUKUDA, *J. Jpn Soc. Tech. Plast.* **5** (36) (1964) 3.
3. Y. YAMADA, *ibid.*, **5** (38) (1964) 183.
4. G. G. MOORE and J. F. WALLACE, *J. Inst. Metals* **93** (1964–1965) 33.
5. D. C. CHIANG and SHIRO KOBAYASHI, *J. Eng. Ind.* November (1966) 443.
6. B. BUDIANSKY and N. M. WANG, *J. Mech. Phys. Solids* **14** (1966) 357.
7. OHWUE TETSURO, TAKECHI HIROSHI and FURUNO YOSHIKUNI, *J. Jpn Soc. Tech. Plast.* **28** No. 314 (1987) 225.
8. S. S. HECKER, M. G. STOUT, K. P. STAUDHAMMER and J. L. SMITH, *Metall. Trans.* **13A** (1982), 619.
9. D. BHANDARKER, V. F. ZACKAY and E. R. PARKER, *ibid.* **3** (1972) 2619.
10. J. P. BRESSANELLI and A. MOSKOWITZ, *Trans. ASM* **59** (1966) 223.
11. P. C. MAXWELL, A. GOLDBERG and J. C. SHYNE, *Metall. Trans.* **5** (1974) 1319.
12. Z. S. BASINSKI and T. E. MITCHELL, *Philos. Mag.* **13** (1966) 103.
13. O. L. De. LANGE, P. J. JACKSON and P. D. K. NATHANSON, *Acta Metall.* **28** (1980) 833.
14. P. J. JACKSON and M. SIEDERSLEBEN, *Scripta Metall.* **18** (1984) 749.
15. A. H. COTTRELL and B. A. BILBY, *Philos. Mag.* **42** (1951) 573.
16. P. L. MANGONON Jr and G. THOMAS, *Met. Trans.* **1** (1970) 1577.
17. J. A. VENABLES, *Philos. Mag.* **6** (1961) 379.

Received 1 September 1993
and accepted 8 September 1994